J. Phys. C: Solid State Phys. **18** (1985) 3175–3189. Printed in Great Britain

Band structures of the layer compounds 1T-TaS_2 and 2H-$TaSe_2$ in the presence of commensurate charge-density waves

N V Smith, S D Kevan and F J DiSalvo
AT&T Bell Laboratories, Murray Hill, New Jersey 07974, USA

Received 22 October 1984

Abstract. Angle-resolved photoemission spectroscopy (ARPES) measurements of the $E(k_\parallel)$ band structure are reported for 1T-TaS_2 and 2H-$TaSe_2$ at temperatures where commensurate CDWs are well developed. Empirical tight-binding calculations of the band structure in the presence of the experimentally known CDW superlattice are also reported. In the case of the $\sqrt{13} \times \sqrt{13}$ CDW in 1T-TaS_2, experiment and theory both reveal a gross distortion of the band structure, in which the Ta-derived d band collapses into three sub-band manifolds separated by gaps. The thirteenth electron is predicted to reside in a conduction band only 50 meV wide, where it is susceptible to a Mott–Anderson transition. In the case of 2H-$TaSe_2$, additional peaks are seen in the ARPES data in the presence of the CDW, but the effects are too weak to distinguish between a band-structure distortion and weak Umklapp associated with the 3×3 superlattice. Calculated densities of states, decomposed according to the inequivalent atomic sites, are presented.

1. Introduction

Work on layer compounds occupies a special place in the history of angle-resolved photoemission spectroscopy (ARPES), since it was on such materials that the utility of ARPES in the direct mapping of band structures was first demonstrated (Smith *et al* 1974, Smith and Traum 1975). In the intervening decade, there have been substantial improvements in the ARPES technique in both energy and momentum resolution (see e.g. Himpsel 1983). The motivation of the present work was to return to the layer compounds and, using a superior ARPES instrument, to study the effects on the band structure of charge-density waves (CDWs) in these materials.

In this paper we report experiments and calculations on the layer compound 1T-TaS_2, which displays a strong CDW, and on 2H-$TaSe_2$, which by way of contrast displays a weak CDW. The superlattice in the case of 1T-TaS_2 has a $\sqrt{13} \times \sqrt{13}$ unit cell rotated 13°54′ with respect to the unreconstructed (or 1×1) unit cell. The superlattice in the case of 2H-$TaSe_2$ has a 3×3 unit cell aligned along the same axes as the 1×1 unit cell.

To assist in the interpretation we have devised simple tight-binding or linear combination of atomic orbitals (LCAO) models. These start by fitting the unreconstructed band structures using a minimal basis set of Ta d orbitals. The band structures in the presence of a CDW are then simulated by selective strengthenings and weakenings of hopping integrals between neighbouring atoms in the superlattice unit cell. The ARPES data as elucidated by the LCAO calculations offer insight into the effects of CDWs on the

0022-3719/85/163175 + 15 $02.25

electronic structure, as well as providing some estimate of the amplitudes of CDWs themselves.

2. Experimental procedure

Our ARPES experiments were performed using a new instrument designed for high resolution in both energy and momentum (Kevan 1983). The source was a resonance lamp providing both He I ($\hbar\omega = 21.22$ eV) and Ne I ($\hbar\omega = 16.85$ eV) photons.

Single-crystal samples were attached using Ag-filled epoxy cement to a sample holder/manipulator which could be cooled to liquid nitrogen temperature. The samples were cleaved in an ultrahigh-vacuum (3×10^{-10} Torr) preparation chamber and checked with low-energy electron diffraction (LEED) for orientation and satisfactory CDW formation. Some difficulty was experienced in getting cooled samples of 1T-TaS_2 to undergo the transformation into the commensurate CDW state. This is attributed to the inhibiting effects of the strains induced by attempting to hold the samples rigorously flat using epoxy cement. Our best results on 1T-TaS_2 were obtained on a sample which may have worked itself partially loose, thereby relieving the inhibiting strains, but leaving some doubt as to whether we have really achieved good flatness and the very high angular resolution of which our instrument is, in principle, capable.

Figure 1 compares two normal emission spectra taken on different samples of 1T-TaS_2 at lowered temperature. In one case the commensurate CDW is well developed and it is seen, in basic agreement with previous observations by Pollak *et al* (1981), that this is accompanied by a strong enhancement of the spectral structure and a downward shift of the peak just below the Fermi level E_F by 0.08 eV. There are three structures in the Ta d-derived region, and these are discernible in both of the spectra of figure 1, and even in room-temperature data (not shown). As we shall discuss below, the existence of more

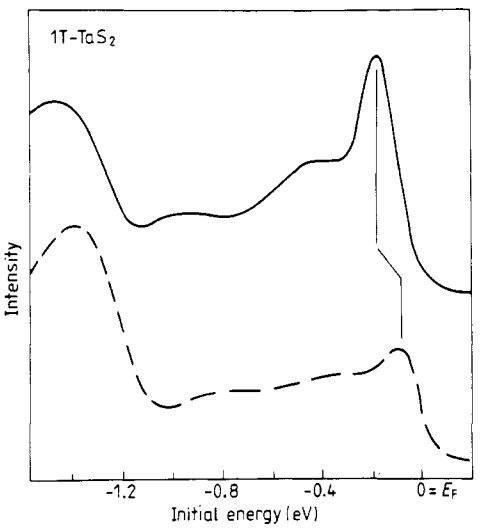

Figure 1. The full (broken) curves show angle-resolved photoemission spectra taken on 1T-TaS_2 in the Ta d-band region in the presence (absence) of a commensurate CDW ($\hbar\omega = 21.2$ eV, $\theta = 0°$).

than one peak in the Ta d-band region is a consequence of the CDW distortion. It is therefore interesting to note that this multiplicity of d-band structures exists irrespective of whether the CDW is commensurate or incommensurate.

3. LCAO band calculations

To interpret the data we have developed simple linear combination of atomic orbitals (LCAO) models. Since we are dealing with superlattices having a large number of atoms per unit cell (39 in the case of 1T-TaS_2), *ab initio* band calculations would be extraordinarily expensive, and this presumably accounts for the absence of such calculations in the literature. Our approach has been to set up the simplest LCAO models which still retain the important features of the known 1×1 band structures. We have striven to keep the number of basis orbitals and the number of free parameters within manageable bounds.

In the case of 1T-TaS_2, we follow Mattheiss (1973) and set up an effective Hamiltonian involving only Ta d orbitals. It is assumed that the parametrisation is capable of absorbing the indirect Ta–ligand–Ta interactions. We make the additional assumptions of strict two-dimensionality (i.e. no interlayer interactions) and nearest-neighbour interactions within the two-centre approximation. The resulting Hamiltonian (Miasek 1957) is listed in table 1 in terms of $\xi(=k_x a/2)$ and $\eta(=\sqrt{3}k_y a/2)$, where a is the lattice parameter. There are only six parameters, the nearest-neighbour hopping integrals ddσ, ddπ and ddδ, and the diagonal energies d_{z^2}, d_{xy} and d_{yz} of the $3z^2 - r^2$, $xy/x^2 - y^2$ and yz/zx orbitals respectively. Note that at this level of approximation, the yz and zx orbitals are decoupled from the other three. Since they reside at energies well above E_F, we can drop them from the basis set and discard the associated parameter d_{yz}.

Table 1. Slater–Koster matrix elements for a two-dimensional hexagonal structure in the two-centre approximation (Miasek 1957). Only non-vanishing elements are listed.

$(3z^2 - r^2/3z^2 - r^2)$	$d_{z^2} + \frac{1}{2}(dd\sigma + 3dd\delta)(2\cos\xi\cos\eta + \cos 2\xi)$
$(x^2 - y^2/x^2 - y^2)$	$d_{xy} + \frac{1}{2}(3dd\sigma + 12dd\pi + dd\delta)\cos\xi\cos\eta + \frac{1}{2}(3dd\sigma + dd\delta)\cos 2\xi$
(xy/xy)	$d_{xy} + \frac{1}{4}(9dd\sigma + 4dd\pi + 3dd\delta)\cos\xi\cos\eta + 2dd\pi\cos 2\xi$
(yz/yz)	$d_{yz} + (3dd\pi + dd\delta)\cos\xi\cos\eta + 2dd\delta\cos 2\xi$
(zx/zx)	$d_{yz} + (dd\pi + 3dd\delta)\cos\xi\cos\eta + 2dd\pi\cos 2\xi$
$(3z^2 - r^2/x^2 - y^2)$	$\frac{1}{2}\sqrt{3}(dd\sigma - dd\delta)(\cos\xi\cos\eta - \cos 2\xi)$
$(3z^2 - r^2/xy)$	$\frac{3}{2}(dd\sigma - dd\delta)\sin\xi\sin\eta$
$(x^2 - y^2/xy)$	$\frac{1}{4}\sqrt{3}(3dd\sigma - 4dd\pi + dd\delta)\sin\xi\sin\eta$
(yz/zx)	$-\sqrt{3}(dd\pi - dd\delta)\sin\xi\sin\eta$

For 1T-TaS_2 a reasonable simulation of the first-principles bands in the vicinity of E_F is obtained by setting the five free parameters as follows: $dd\sigma = -0.05483$, $dd\pi = 0.01769$, $dd\delta = 0.00802$, $d_{z^2} = 0.4698$ and $d_{xy} = 0.4653$; energies are expressed in Rydbergs, and E_F occurs at 0.3753 Ryd. The bands are shown in figure 2(*a*).

In the case of 2H-$TaSe_2$ our abbreviated Hamiltonian is not sufficiently flexible to reproduce the precise shape of the occupied d band. This difficulty does not occur in LCAO models with the full three-centre parametrisation (Mattheiss 1973) or a basis set including the ligand orbitals (Doran and Woolley 1981). Rather than go to these lengths,

we have moved in the opposite direction, towards further simplification. The average energy of the $xy/x^2 - y^2$ manifold relative to the $3z^2 - r^2$ band lies higher in the 2H polytype with respect to the 1T polytype (Mattheiss 1973). We therefore seek a model based on the $3z^2 - r^2$ orbital alone. Such a model, having sufficient fitting flexibility, can be set up, provided one includes second and third neighbours. The band energy is given by

$$E_{z^2} = \mathrm{d}_{z^2} + d_1(2\cos\xi\cos\eta + \cos 2\xi) + d_2(2\cos 3\xi\cos\eta + \cos 2\eta) + d_3(2\cos 2\xi\cos 2\eta + \cos 4\xi). \quad (1)$$

The coefficients d_n are equal to $\frac{1}{2}(\mathrm{dd}\sigma_n + 3\mathrm{dd}\delta_n)$ where the index $n = 1, 2, 3$ runs over first-, second- and third-nearest neighbours respectively. It would be more appropriate, however, to regard d_1, d_2 and d_3 as adjuncts of the fitting scheme, rather than imbuing them with any literal physical significance.

A reasonable simulation of the band structure of 2H-$TaSe_2$ obtained by setting d_1, d_2 and d_3 equal to 0.1900, 0.4700 and 0.0322 eV respectively is shown in figure 2(*b*). These parameters were obtained by first fitting the first-principles results and then stretching the band by about a factor of 2 in order to produce an occupied d-band width (~0.5 eV) in closer agreement with the photoemission data. Note particularly the excursion of the band below E_F midway along the ΓK symmetry line. It is this feature which cannot be reproduced by the Hamiltonian of table 1, but is important because it occurs in all first-principles calculations, and is observable experimentally.

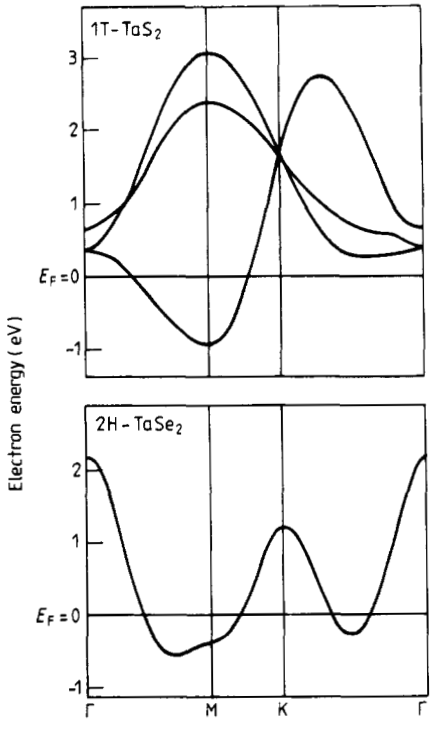

Figure 2. Empirical band structures of 1T-TaS_2 and 2H-$TaSe_2$ in the unreconstructed state.

To simulate the effects of CDWs on the band structure, the Hamiltonian of table 1 or of equation (1) is opened out (unfolded?) into the larger unit cell of the superlattice. X-ray diffraction work by Brouwer and Jellinek (1980) indicates that the atomic displacements associated with the CDW can be pictured in terms of 7-atom or 13-atom Ta clusters. The effects on the band structure are calculated by assuming that the interatomic hopping integrals ddσ, ddπ and ddδ scale as D^{-5}, where D is the appropriate Ta–Ta interatomic distance. Our method is the same as that used by Doran and Woolley (1981), but it has been stripped to its barest essentials. By restricting the number of basis orbitals, the superlattice Hamiltonian matrix can be kept conveniently small, being 39 × 39 for 1T-TaS_2 and 9 × 9 for 2H-$TaSe_2$. Figure 3 provides a foretaste, in the case of 1T-TaS_2, of how the density of states is modified in the presence of a commensurate CDW.

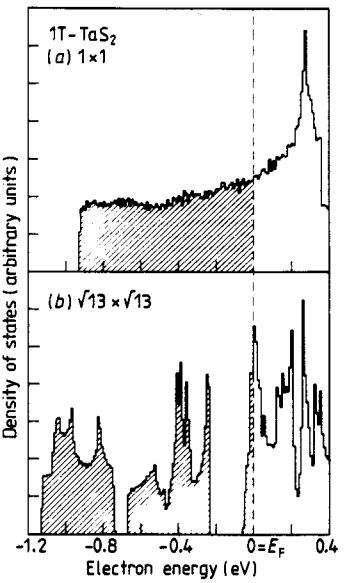

Figure 3. Calculated Ta d-band density of states: (*a*) in the absence, (b) in the presence of a commensurate CDW.

4. 1T-TaS_2: results and discussion

4.1. ARPES data

Photoemission spectra taken on 1T-TaS_2 in the ΓM azimuth as a function of angle of emission θ with respect to the surface normal are shown in figure 4. Three structures are seen in the Ta d-band region at approximately −0.2 eV, −0.5 eV and −1.0 eV relative to E_F. (The peak seen at −1.4 eV for $\theta = 0°$ is associated with the S-derived p band, and will not be discussed in this paper.) The main intensity shifts between the three d features, but there is little energy dispersion compared with the separation of the peaks.

The observation of three d peaks is in flat contradiction with the expectations of the unreconstructed band structure of figure 2(*a*), which permits only one occupied d band. Our spectra along the ΓK azimuth (not shown) are rather similar to those along ΓM,

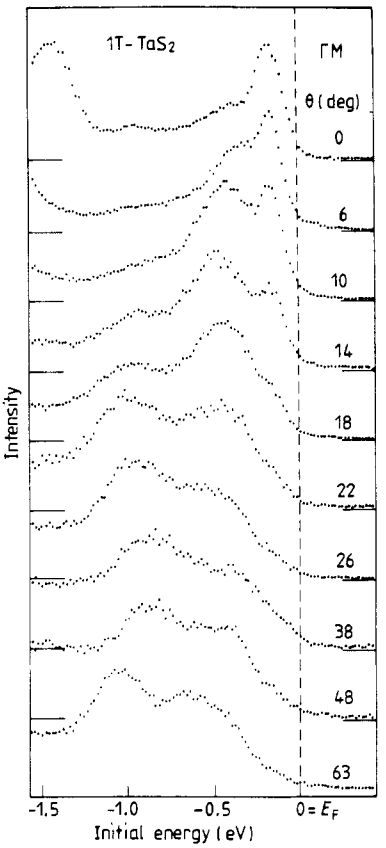

Figure 4. Angle-resolved photoemission spectra on 1T-TaS_2 in the presence of a commensurate CDW taken as a function of polar angle of emission θ ($\hbar\omega = 21.22$ eV, ΓM azimuth).

which is also in contradiction with the prediction of the unreconstructed band structure. A number of authors have noted the existence of forbidden d emission along the ΓK azimuth (Smith and Traum 1975, Mamy *et al* 1981).

4.2. CDW Structure

The $\sqrt{13} \times \sqrt{13}$ unit cell of 1T-TaS_2 in the presence of a commensurate CDW is shown in figure 5. There are three types of inequivalent atoms designated a, b and c in the numerical proportion 1:6:6. The atomic displacements are characterised as a contraction of the seven-atom cluster comprising an atom of type a and its surrounding b atoms (Brouwer and Jellinek 1980). The ab distance decreases by 6.4%. The c atoms also move towards the nearest a atom—the bc distance decreases by 3.2%—so that we may speak of 13-atom 'Star-of-David' clusters. We have used only the simplest representation of this structure. In particular, we have ignored the slight non-radial movements of atoms b and c with respect to the cluster. We have also ignored interlayer interactions which can also remove the strict equivalence within the b and c atom subsets (Naito *et al* 1983).

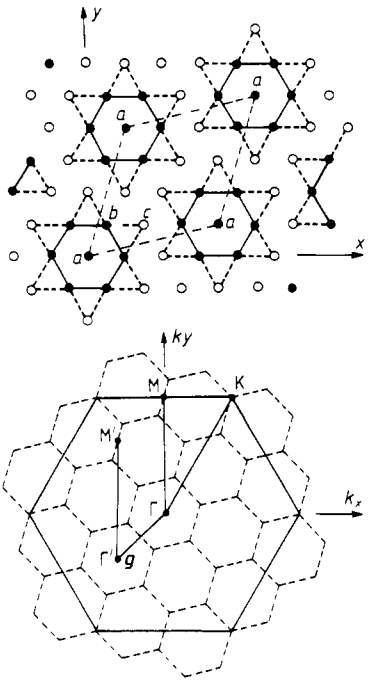

Figure 5. Real-space unit cell and Brillouin zone for the $\sqrt{13} \times \sqrt{13}$ superlattice in 1T-TaS_2.

Figure 5 shows the Brillouin zones for both the 1×1 and $\sqrt{13} \times \sqrt{13}$ structures. In this paper we shall present results exclusively in terms of the 1×1 Brillouin zone since this corresponds more closely to our experimental procedure.

4.3. Comparison between experiment and theory

We first investigate whether the ARPES data could be understood in terms of Umklapp, i.e. weak Bragg diffraction through reciprocal-lattice vectors of the CDW superlattice. For example, if we have set the sample and analyser so as to scan along ΓM we are simultaneously scanning along the ΓM′ shown in figure 5(*b*). Electrons optically excited on this line can scatter into our line of sight by diffraction through the vector $-\boldsymbol{g}$.

Figure 6(*a*) shows (broken curves) the superposition of all additional bands derived from such Umklapp process. It should be evident that weak Umklapp is unable to explain even the qualitative features of the ARPES data.

Inclusion of the CDW atomic displacements has the effect of removing many of the band crossings, and the consequences of the D^{-5} law are shown in figure 6(*b*). There is a gross distortion of the original band structure. In the occupied region the bands collapse into three sub-manifolds separated by gaps: (1) a narrow (50 meV wide) manifold immediately below E_F; (2) a middle three-band manifold in the range -0.23 to -0.67 eV; (3) a lower three-band manifold in the range -0.74 to 1.13 eV. The lower and middle manifolds are completely occupied containing six electrons each. The remaining (thirteenth) Ta d electron populates the upper manifold, placing E_F only 50 meV above the bottom of the conduction band.

The positions of the peaks in the experimental ARPES data have been superimposed on figure 6(*b*). The two lower peaks in the data can be immediately identified with the lower and middle manifolds in the theoretical calculations. The mean energy positions and the extent of the energy dispersion are in good agreement. There are differences in the shape of the dispersion which we attribute to the main weight of the observed peak passing back and forth between the three bands within each manifold.

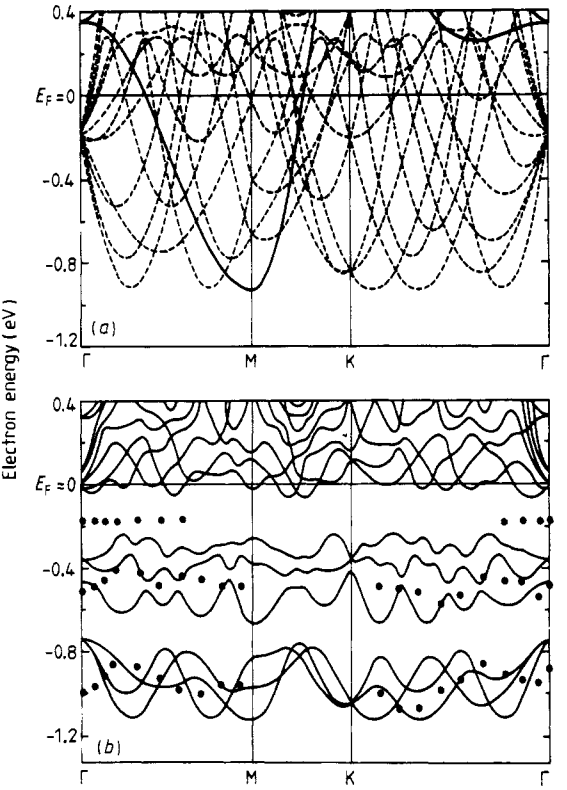

Figure 6. $E(k_{\|})$ dispersion relations for 1T-TaS_2: (*a*) band structure of the unreconstructed crystal (full curves), and superlattice Umklapp bands (broken curves) derived by translation through reciprocal-lattice vectors of the $\sqrt{13} \times \sqrt{13}$ unit cell; (*b*) experimental band-structure results (full circles) are compared with calculated bands (full curves) which incorporate effects due to CDW atomic displacements. ΓM and MKΓ correspond to symmetry directions in the Brillouin zone of the unreconstructed crystal.

There are two choices for the assignment of the uppermost experimental peak. First, if we identify it with the narrow uppermost theoretical manifold, we need to explain why it moves so far from E_F when the CDW is fully developed. Following Fazekas and Tosatti (1980) we may conjecture that the reconstructed system is unstable against a Mott or Anderson transition which opens up an additional gap at E_F. As emphasised by Fazekas and Tosatti, it is not the Mott transition which drives the reconstruction; rather, it is the

reconstruction which brings about favourable conditions for the Mott transition to take place.

In the second and alternative assignment, we identify the uppermost experimental peak as part of the middle manifold whose upper edge lies only 0.1 eV lower (not a major discrepancy given the crudity of the theoretical calculations). We would then have to propose that there exists an as yet undetected narrow 'metallic' peak at E_F. There is a very suggestive similarity here with the situation on the 7×7 reconstructed surface of Si(111). That system has a metallic surface state which has been associated recently with a very narrow band which dominates the low-frequency behaviour (Demuth *et al* 1983). At present we cannot distinguish between these alternative interpretations on the basis of ARPES data. The long established semiconducting behaviour of 1T-TaS_2 at low temperatures clearly favours the Mott–Anderson interpretation.

We conclude that the band theory with inclusion of CDW distortions is quite successful. It accounts nicely for the principal, and previously unexplained, experimental result that the d band collapses into a number of sub-manifolds separated by gaps. Note that the CDW distorted bands are relatively isotropic, also in agreement with experiment. Some discrepancies remain, which is perhaps not too surprising in view of the lack of sophistication in the theory. Calculations using more powerful techniques would be welcome.

4.4. Densities of states

The density of states (DOS) calculated in both the presence and absence of the CDW distortions has been shown above in figure 3. In the presence of the CDW, E_F falls close to the maximum of a sharp peak in the DOS. This, combined with the narrow width (50 meV) of the occupied region and low electron density in the conduction band (one electron per 13 Ta atoms), lends support to the notion of a Mott transition.

The atom-by-atom decomposition of the DOS is shown in figure 7. For electrons in the lower manifold, the DOS is largest for atoms of type a, whereas in the middle manifold it is largest for atoms of type b. The total numbers of occupied electrons per atom on atoms of type a, b and c are $n_a = 1.455$, $n_b = 1.311$ and $n_c = 0.611$. These numbers should not be interpreted literally, since self-consistent first-principles calculations would be required for that. Some semiquantitative conclusions can be drawn.

First, the charge transfers involve a substantial fraction of an electron per atom. The ARPES data therefore support those who propose that the CDW has a relatively large amplitude (Wilson 1978).

Secondly we find that $(n_a - n_b) \ll (n_b - n_c)$, implying that the CDW has a fairly uniform amplitude within the seven-atom cluster. This result serves to explain the failure to resolve a separate a-atom feature in Mössbauer data (Pfeiffer *et al* 1984) and core-level x-ray photoemission spectra (Wertheim *et al* 1975, Hughes and Pollak 1976, Pollak *et al* 1981). In the x-ray photoemission data of Pollak *et al* (1981) on 1T-TaS_2 in the presence of the commensurate CDW, two 4f core-level peaks are observed showing a separation of 0.73 eV which is interpreted as the chemical shift between atoms of types b and c. Taking the ratio between $(n_a - n_b)$ and $(n_b - n_c)$ literally, we estimate that the chemical shift between atoms a and b should be 0.15 eV towards lower binding energy which is smaller than the 0.25 eV core linewidth. NMR measurements on 1T-TaS_2 reveal more than three inequivalent Ta sites, suggesting that the sixfold b and c sets should be further subdivided in the ratio 2:2:2 (Naito *et al* 1983). Such distinctions appear to be beyond the sensitivity of current ARPES and core-level XPS experiments.

Our results, that n_a and n_b are very close, are inconsistent with a purely sinusoidal

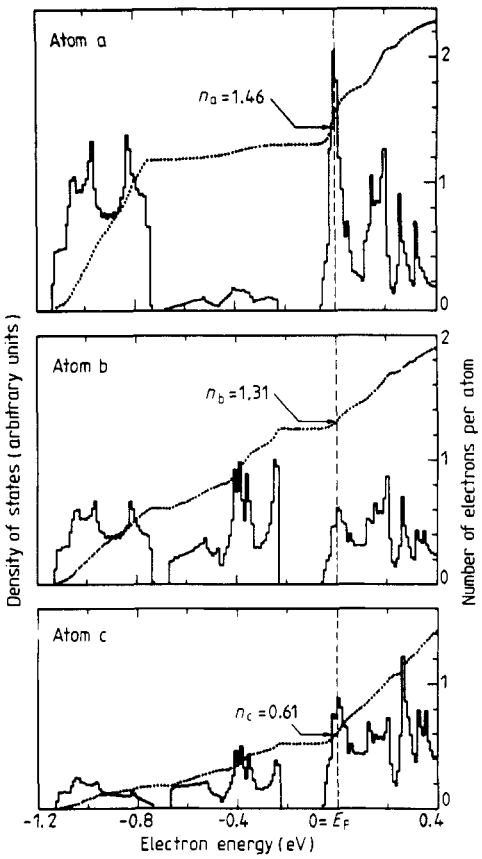

Figure 7. Calculated densities of states for 1T-TaS_2 for each of the inequivalent atoms in the $\sqrt{13} \times \sqrt{13}$ unit cell.

CDW since that would require a considerably greater charge surfeit on atom a (Wilson 1978). It is also inconsistent with the detailed model of Fazekas and Tosatti (1980) which proposes a charge depletion on atom a. Our empirical LCAO calculations indicate that the charge of the 'thirteenth' electron of the conduction band is distributed 14%, 5% and 9% on atoms a, b and c respectively.

4.5. Joint density of states

A joint density of states was generated using the CDW distorted band structure, and the results are compared in figure 8 with the infrared absorption data of Barker *et al* (1975). The step in the $\hbar\omega = 0.2$–0.4 eV range is attributed to the onset of transitions between states in the intermediate manifold of figure 6(*b*) and states above E_F.

The experimental data show a weak peak at ~0.1 eV. A peak is seen at this energy in the joint density of states, and corresponds exclusively to transitions from initial states in the 50 meV-wide conduction band. The available infrared absorption data therefore lend some support to the proposed existence of a 'metallic'band in 1T-TaS_2 (one of the alternatives discussed in § 4.3 above), but it should be emphasised that the experimental feature is uncertain.

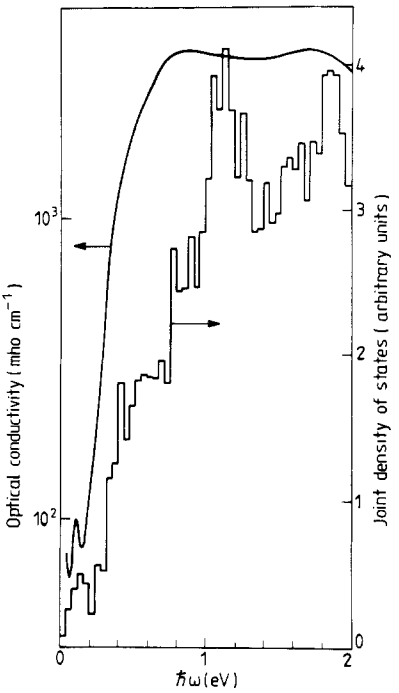

Figure 8. Joint density of states for $\sqrt{13} \times \sqrt{13}$ 1T-TaS_2 is compared with the infrared absorption data of Barker *et al* (1975).

5. 2H-$TaSe_2$: results and discussion

5.1. ARPES data

Photoemission spectra taken on 2H-$TaSe_2$ in the ΓM and ΓK azimuths as a function of θ are shown in figure 9. On increasing θ we observe in both azimuths a prominent Ta d-derived peak (designated P) which appears just below E_F, disperses down to a minimum energy, disperses upwards and then crosses E_F. The behaviour, however, is quantitatively different for the two azimuths in terms of $k_\parallel$ range and extent of dispersion. This anisotropy (which is real and cannot be attributed to the different photon energies used in figures 9(*a*) and 9(*b*)) is in contrast with the behaviour observed in 1T-TaS_2.

In addition to the prominent peak, a weaker feature (designated W) is discerned in most of the spectra. It shows little if any dispersion.

5.2. CDW structure

The 3 × 3 unit cell of 2H-$TaSe_2$ in the presence of the commensurate CDW is shown in figure 10. There are three types of inequivalent atoms designated a, b and c in the numerical proportions 1:6:2. According to x-ray diffraction and neutron diffraction measurements, the atomic displacements can once again be characterised as an internal contraction of the seven-atom cluster comprising an atom of type a and its six surrounding b atoms. We have used a simplified structure extracted from the essentials of the available structural information using the 'ideal' case (phase $\varphi = 120°$ in the terminology of

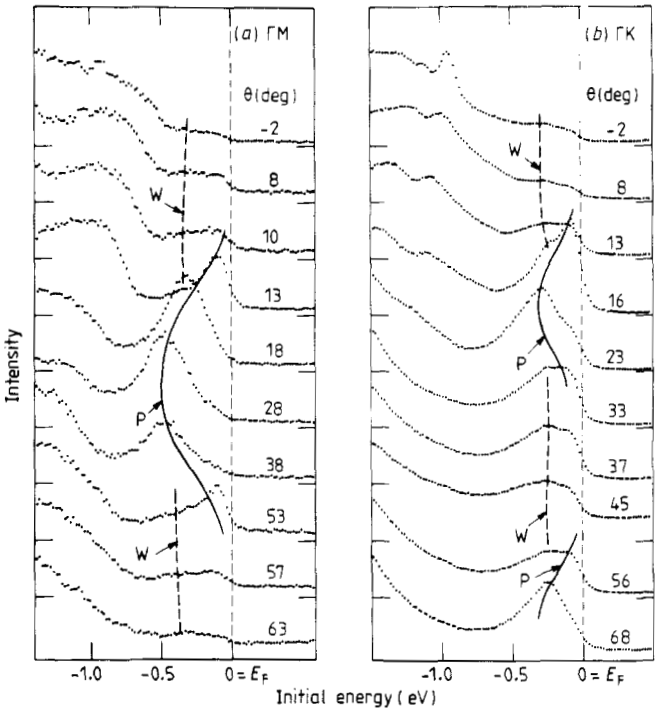

Figure 9. Angle-resolved photoemission spectra on 2H-$TaSe_2$ in the presence of a commensurate CDW taken as a function of polar angle θ: (*a*) ΓM azimuth, $\hbar\omega = 21.22$ eV; (*b*) ΓK azimuth, $\hbar\omega = 16.85$ eV.

Wilson 1978). Following Brouwer and Jellinek (1980), we have adopted the cluster as opposed to the sign-reversed and experimentally indistinguishable structure proposed by Moncton *et al* (1977) based on neutron scattering. Moncton *et al* place a lower limit of 2.1% on the contraction of the a–b distance. Using the D^{-5} scaling of the hopping parameters d_1, d_2 and d_3 leads to a rather small effect on the model band structure. For illustrative purposes, we have therefore used a doubled contraction of 4.2% rather than the 2.1% lower limit. Our results are similar in their essentials to those of Doran and Woolley (1981).

Figure 10 shows the Brillouin zones for both the 1×1 unreconstructed and 3×3 superlattice structures. As throughout, we shall refer results to the 1×1 Brillouin zone.

5.3. Comparison between experiment and theory

The experimental $E(k_\parallel)$ data associated with peak P and weaker feature W are compared with the model band structures in figure 11. The comparison of figure 11(*a*) shows the 1×1 band structure (full curves) and the Umklapp shifted bands (broken curves) associated with the 3×3 superlattice. The comparison of figure 11(*b*) superimposes the same experimental data on the model bands in the presence of CDW distortion associated with a 4.2% contraction of the a–b distance.

We find qualitative $E(k_\parallel)$ agreement in that the strong experimental feature (peak P) follows the behaviour of the 1×1 band structure (a downward excursion along ΓM

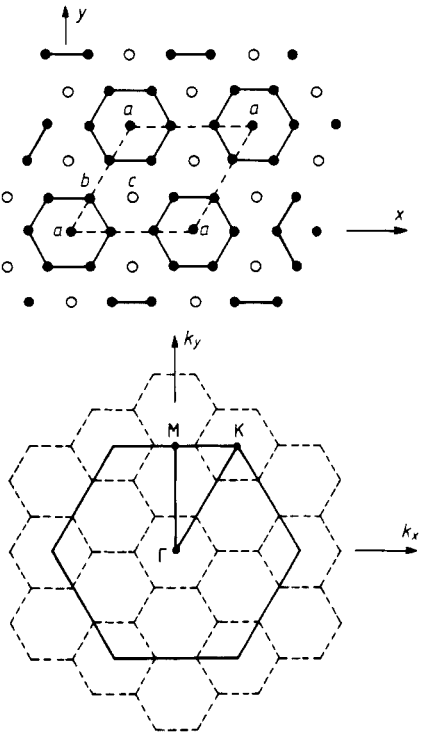

Figure 10. Real-space unit cell and Brillouin zone for the 3 × 3 superlattice in 2H-$TaSe_2$.

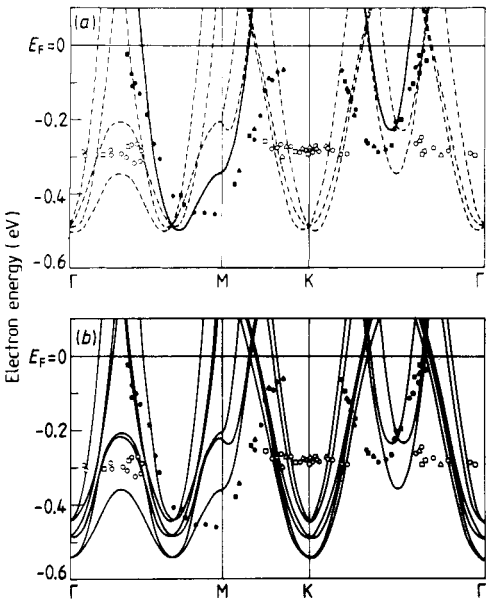

Figure 11. Experimental $E(k)$ results 2H-$TaSe_2$ are compared with theory. Full and open symbols correspond to features P and W of figure 9 respectively. (*a*) Unreconstructed bands (full curves) and superlattice Umklapp bands (broken curves). (*b*) Bands in the presence of a 3 × 3 CDW.

with a minimum near M, and also an excursion below E_F somewhere midway along ΓK). Inclusion of superlattice effects accounts for the existence of the weaker experimental feature W.

Quantitative aspects of the agreement are not impressive. We have previously mentioned the need to stretch the width of the Ta d band generated by first-principles calculations by about a factor of two. Details of the $E(k_\parallel)$ dispersion of the weak feature W are not well reproduced. Nor is the agreement significantly improved by explicit inclusion of the CDW distortion (compare figures 11(*a*) and 11(*b*)). We advance as the main reason for this lack of detailed agreement our neglect of the interlayer interactions. It should be emphasised that the occupied width of the Ta d band is only 0.5 eV experimentally, and considerably less theoretically. Differences in energies between the ΓMK-based plane and the ALH plane of the three-dimensional Brillouin zone can be relatively large. We conclude that the modest measure of agreement in figure 11 is about as good as can be expected given the present resolution of the experiment and the approximations in the theory. A CDW superlattice *is* required to explain the existence of weak feature W, but the ARPES data are not sufficiently incisive to give an estimate of the CDW amplitude.

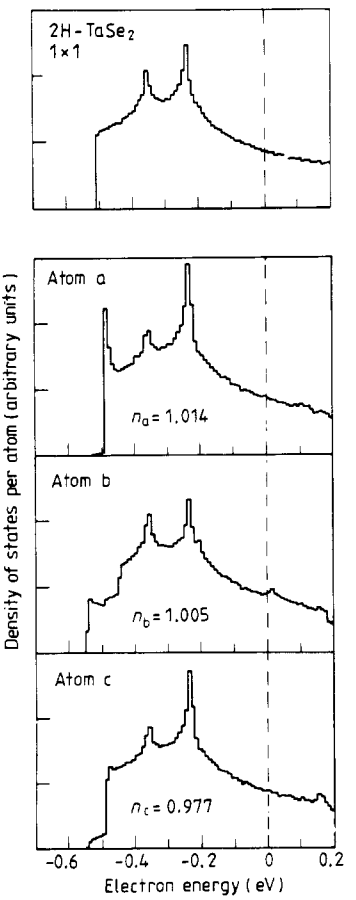

Figure 12. Calculated density of states for 2H $TaSe_2$ in both unreconstructed states and for each of the inequivalent atoms in the 3 × 3 reconstructed state.

5.4. Densities of states

The calculated density of states of 2H-$TaSe_2$ is shown in figure 12 for the unperturbed (1×1) case and, decomposed according to inequivalent a, b, c atoms, for the case in the presence of the (3×3) CDW distortion (4.2% contraction of the a–b distance). In contrast with 1T-TaS_2 the results are not dramatic; no gaps appear. The main differences occur at the bottom of the occupied d bands, in particular the singularity at -0.48 eV in the a atom density of states. The numbers of Ta d electrons on each of the inequivalent sites are $n_a = 1.014$, $n_b = 1.005$ and $n_c = 0.977$. The departures from unity are relatively small, although once again we have $(n_a - n_b) < (n_b - n_c)$. We conclude that CDW effects on the band structure of 2H-$TaSe_2$ (even after the deliberate exaggerations of our LCAO model) are weak compared with the dramatic effects in 1T-TaS_2.

Acknowledgments

We have benefited from discussions with M Eibschutz, L F Mattheiss and L Pfeiffer.

References

Barker A S Jr, Ditzenberger J A and DiSalvo F J 1975 *Phys. Rev.* B **12** 2049
Brouwer R and Jellinek F 1980 *Physica* B **99** 51
Demuth J E, Persson B N J and Schell-Sorokin A J 1983 *Phys. Rev. Lett.* **51** 2214
Doran N J and Woolley A M 1981 *J. Phys. C: Solid State Phys.* **14** 4257
Fazekas P and Tosatti E 1980 *Physica* B **99** 183
Himpsel F J 1983 *Adv. Phys.* **32** 1
Hughes H P and Pollak R A 1976 *Phil. Mag.* **34** 1025
Kevan S D 1983 *Rev. Sci. Instrum.* **54** 1441
Mamy R, Thiry P, Vachier G and Couget A 1981 *J. Physique* **42** L79
Mattheiss L F 1973 *Phys. Rev.* B **8** 3719
Miasek M 1957 *Phys. Rev.* **107** 92
Moncton D E, Axe J D and DiSalvo F J 1977 *Phys. Rev.* B **6** 801
Naito M, Nishihara H and Tanaka S 1983 *J. Phys. C: Solid State Phys.* **16** L387
Pfeiffer L, Kovacs T and DiSalvo F J 1984 *Phys. Rev. Lett.* **52** 687
Pollak R, Eastman D E, Himpsel F J, Heimann P and Reihl B 1981 *Phys. Rev.* B **24** 7435
Smith N V and Traum M M 1975 *Phys. Rev.* B **11** 2087
Smith N V, Traum M M and DiSalvo F J 1974 *Solid State Commun.* **15** 211
Wertheim G K, DiSalvo F J and Chiang S 1975 *Phys. Lett.* **54A** 304
Wilson J A 1978 *Phys. Rev.* B **17** 3880